Thermochimica Acta 511 (2010) 112–118

Contents lists available at ScienceDirect

Thermochimica Acta

journal homepage: www.elsevier.com/locate/tca

Preparation, characterization and catalytic behavior of $CdFe_2O_4$ and Cd nanocrystals on AP, HTPB and composite solid propellants, Part: 79

G. Singh*, I.P.S. Kapoor, Reena Dubey, Pratibha Srivastava

Department of Chemistry, D.D.U. Gorakhpur University, Gorakhpur 273009, Uttar Pradesh, India

ARTICLE INFO

Article history:
Received 8 May 2010
Received in revised form 29 July 2010
Accepted 1 August 2010
Available online 8 August 2010

Keywords:
Composite solid propellants
Burning rate
Ammonium perchlorate
Catalytic activity
Ignition delay

ABSTRACT

$CdFe_2O_4$ and Cd nanocrystals were synthesized by wet chemical and hydrazine reduction methods, respectively. These nanocrystals were characterized by XRD and TEM. Their catalytic activity was investigated on the thermal decomposition of ammonium perchlorate (AP), hydroxyl terminated polybutadiene (HTPB) and composite solid propellants (CSPs) using TG and TG-DSC. Burning rate of CSPs was considerably enhanced by these nanocrystals. Rapid thermolysis of the CSPs and AP has also been studied using ignition delay measurements.

1. Introduction

Nanotechnology is the understanding and control of matter at dimensions of roughly 1–100 nm where unique phenomena enable novel applications [1]. Nanosized particles show catalytic activity different from those of conventional bulk materials due to their extremely small size or large surface area [2,3].

A burst of research activity is witnessed in recent years in the area of synthesis and fabrication of different size and shape of metal nanoparticles by hydrazine reduction method [4–7]. Cadmium nanoparticles have been utilized as catalysts, conducting and magnetic materials.

Similarly synthesis of nanosized spinel ferrite particles has become an important part of modern ceramic research. Study of nanosized spinel ferrite has great relevance to modern technology [8]. The wet-chemical synthesis of high reactive powders has been proved to be one of the most effective routes to decrease the sintering temperature of ferrites. $CdFe_2O_4$ has a normal spinel structure similar to $ZnFe_2O_4$, and has been categorized as an antiferromagnet [9].

Composite solid propellants (CSPs) are the major source of chemical energy in space vehicles and missiles. AP is the key energetic material and the most common oxidizer in the burning process. Thermal decomposition characteristics of AP influence the combustion behavior of the propellants. Recent investigations have shown that the pure metal and ferrite nanoparticles are effective to improve the thermal decomposition efficiency of AP [10,11]. In the present work, Cd and $CdFe_2O_4$ nanoparticles are prepared by hydrazine reduction and wet chemical method, respectively. The prepared nanoparticles were further characterized and used to improve the thermal decomposition properties of AP and AP/HTPB (hydroxyl terminated polybutadiene).

2. Experimental

2.1. Materials

Chemical reagents $CdCl_2{\cdot}H_2O$, $FeCl_3$, NaOH, Ethylene glycol, $N_2H_4{\cdot}H_2O$, AP, HTPB, IPDI and DOA were used without further purification.

2.2. Preparation of $CdFe_2O_4$ and Cd

0.4 M (25 mL) of $FeCl_3$ and 0.2 M (25 mL) $CdCl_2{\cdot}H_2O$ were mixed in double distilled, de-ionized water. 3 M (25 mL) solution of NaOH was prepared and slowly added to the solution. The reactants were constantly stirred using a magnetic stirrer until a pH level of 11–12 was reached. The viscous precipitate were then brought to a reaction temperature of 80 °C and stirred for 1 h and washed with distilled water followed by ethanol. The black colored precipitate were then dried overnight at 100 °C and calcined at 300 °C for 3 h.

$CdCl_2{\cdot}H_2O$ (25 mg) was dissolved in ethylene glycol followed by addition of 0.05 M hydrazine. 1.0 M NaOH solution was then added

* Corresponding author. Tel.: +91 551 2202856; fax: +91 551 2340459.
E-mail address: gsingh4us@yahoo.com (G. Singh).

0040-6031/$ – see front matter © 2010 Elsevier B.V. All rights reserved.
doi:10.1016/j.tca.2010.08.001

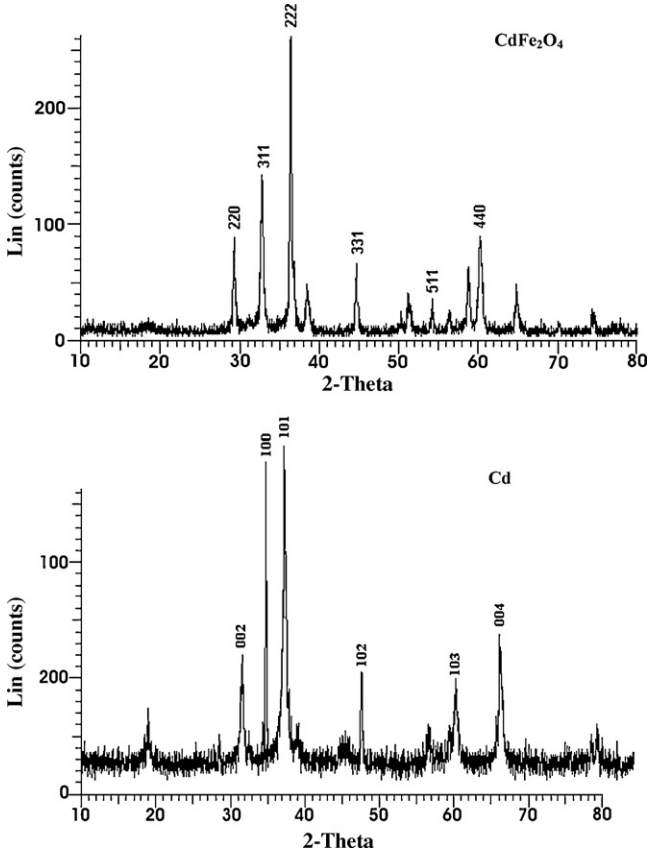

Fig. 1. XRD of $CdFe_2O_4$ and Cd nanocrystals.

to this solution. At a temperature of 60 °C, Cd nanocrystals were formed after about 1 h with magnetic stirring [12].

2.3. Characterization of $CdFe_2O_4$ and Cd

The prepared nanocrystals were characterized for their phase purity and crystallinity by powder X-ray diffraction (Bruker AXSD8 advance) using Cu-Kα (λ = 1.5418 Å) radiation (Fig. 1). The particle size and morphology were investigated by transmission electron microscope (TEM) model Hitachi (H-7500) 120 KV (Fig. 2).

3. Preparation of CSPs

CSPs samples were prepared by dry mixing [13] of AP [100–200 mesh] with $CdFe_2O_4$ or Cd nanocrystals (1% by wt), the solid materials were mixed with HTPB in the ratio of 3:1. The binder part includes the curing agent (IPDI) in equivalent ratio to HTPB and plasticizer (DOA, 30% to HTPB). During mixing of the solid components with HTPB, temperature was maintained at 60 °C for 1 h. The propellants were prepared with and without nanocrystals, casted into aluminum plates having dimensions 1 cm × 3 cm × 10 cm. The samples were cured in an incubator at 70 °C for 8–10 days [14].

4. Catalytic activity

4.1. Thermal decomposition

Thermal decomposition was investigated as follows.

4.1.1. Simultaneous TG-DSC

TG-DSC thermogram (Fig. 3) on pure AP and AP with $CdFe_2O_4$ and Cd nanocrystals (by mixing in ratio of 99:1) were recorded on the samples (~12 mg) using PerkinElmer (Pyris Diamond) under

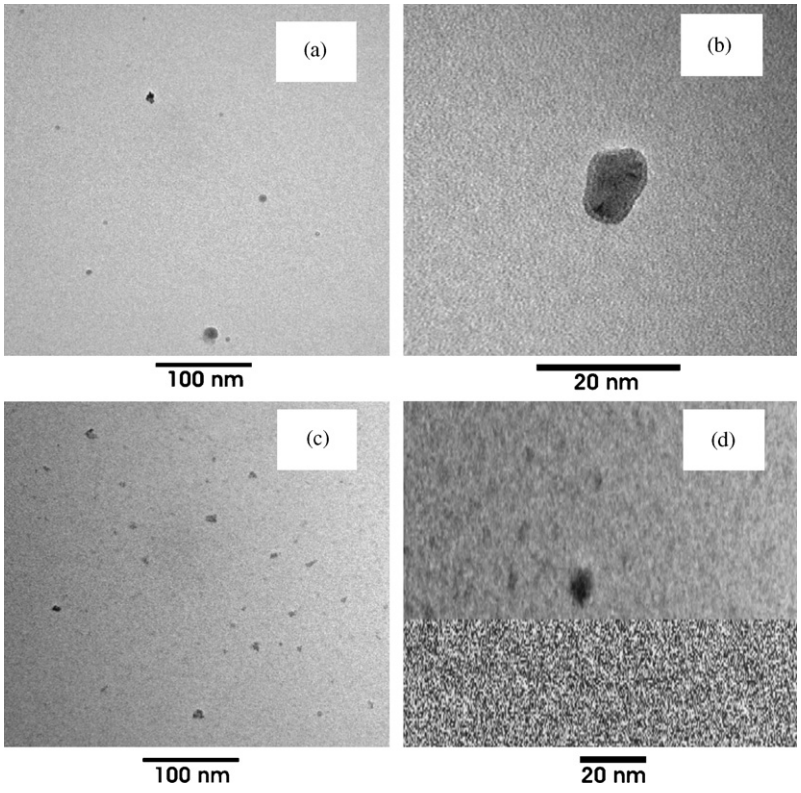

Fig. 2. TEM image of $CdFe_2O_4$ (a and b) and Cd (c and d) nanocrystals.

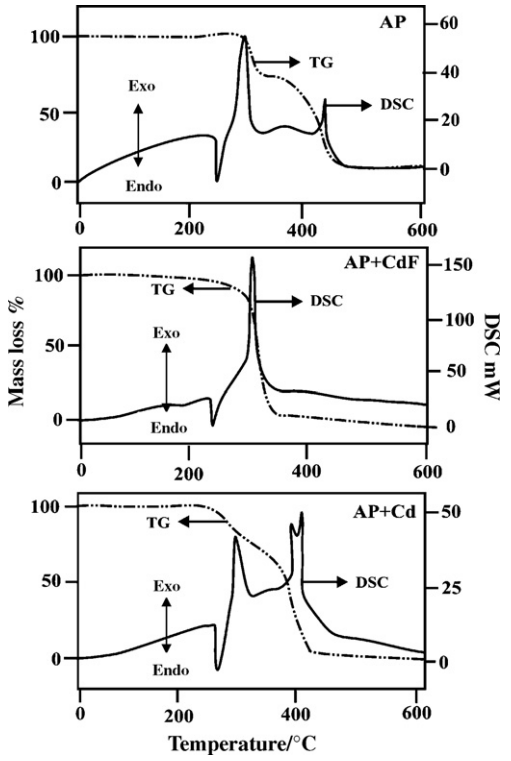

Fig. 3. TG-DSC curves of AP with and without 1% $CdFe_2O_4$ (CdF) and Cd nanocrystals in nitrogen atm.

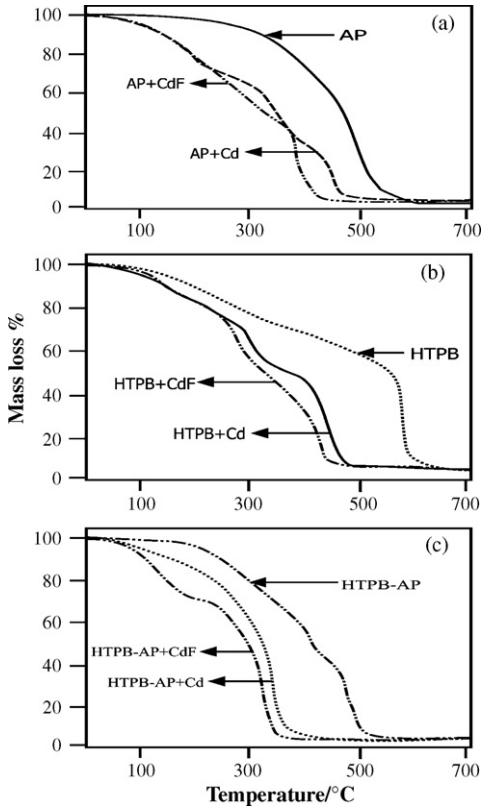

Fig. 4. Non-isothermal TG curve of (a) AP, (b) HTPB, and (c) HTPB-AP with 1% $CdFe_2O_4$ (CdF) and Cd.

nitrogen atmosphere (flow rate 200 ml/min) at a heating rate of 10 °C min^{-1} in a open alumina pan.

4.1.2. Non-isothermal TG in static air

Non-isothermal TG studies on AP, HTPB and CSPs with and without nanocrystals (wt ~20 mg) were undertaken in static air at the heating rate of 10 °C min^{-1} using an indigenously fabricated TG apparatus [15]. A round bottom gold crucible was used as the sample holder. The percentage mass loss has been plotted against temperature (°C), and the curves are shown in Fig. 4(a–c).

4.1.3. Isothermal TG

The isothermal TG of AP with and without nanocrystals (wt ~20 mg) was taken in static air using the above said TG apparatus at appropriate temperatures (Fig. 5). The isothermal TG of AP by incorporating varied amount of nanocrystals (0.5, 1, 2 and 5% by mass) was also done at 300 °C (Fig. 6).

4.1.4. Kinetic analysis of isothermal TG data

Kinetic analysis of thermal decomposition of AP is usually based on a single-step kinetic Eq. (1) [16]

$$\frac{d\alpha}{dt} = k(T)f(\alpha) \quad (1)$$

where t is the time, T is the temperature, α is the extent of conversion ($0 < \alpha < 1$), $k(T)$ is the rate constant, and $f(\alpha)$ is the reaction model [16], which describes the dependence of the reaction rate on the extent of reactions. The value of α is experimentally derived from the global mass loss in TG experiments. The reaction model may take various forms. The temperature dependence of $k(T)$ can be satisfactorily described by the Arrhenius equation, when substitution into Eq. (1) yields

$$\frac{d\alpha}{dt} = A\exp\left(\frac{-E}{RT}\right)f(\alpha) \quad (2)$$

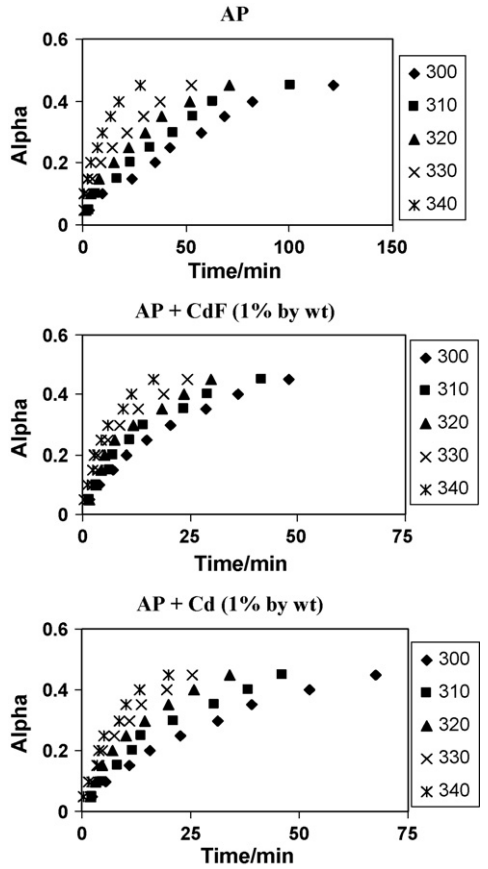

Fig. 5. Isothermal TG of AP, AP + $CdFe_2O_4$ (1% by wt) and AP + Cd (1% by wt) on different temperatures.

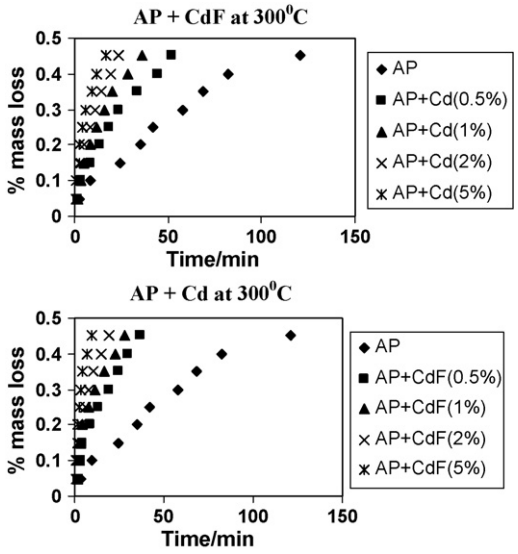

Fig. 6. Isothermal TG of AP with and without $CdFe_2O_4$ (CdF) and Cd nanocrystals on 300 °C.

where A is pre-exponential factor, E the activation energy and R is the gas constant.

4.1.4.1. Model fitting method. Rearrangement and integration of Eq. (1) for isothermal conditions gives

$$g_j(\alpha) = k_j(T)t \tag{3}$$

where $g(\alpha) = \int_0^\alpha [f(\alpha)]^{-1} d\alpha$ is the integrated form of the reaction model. The subscript j has been introduced to emphasize that substituting a particular reaction model in Eq. (3) results in evaluating the corresponding rate constant, which is determined from the slope of a plot of $g_j(\alpha)$ verses t. For each reaction model selected, the rate constants are evaluated at several temperatures T_i and Arrhenius parameters are determined using the Arrhenius Eq. (4) in its logarithmic form

$$\ln k_j(T_i) = \ln A_j - \frac{E_j}{RT_i} \tag{4}$$

Arrhenius parameters were evaluated for isothermal experimental data by the model fitting method.

4.1.4.2. Isoconversional method. This method allows the activation energy to be evaluated without making any assumptions about the reaction model. Additionally, the method evaluates the effective activation energy as a function of the extent of conversion which allows one to explore multistep kinetics.

The basic assumption of the isoconversional method [17] is that the reaction model as defined in Eq. (1) is not dependent on temperature or heating rate. Under isothermal conditions, on combining Eqs. (3) and (4) we get

$$-\ln t_{\alpha,i} = \ln\left[\frac{A_\alpha}{g(\alpha)}\right] - \frac{E_a}{RT_i} \tag{5}$$

where E_α is evaluated from the slope of the plot of $-\ln t_{\alpha,i}$ against T_i^{-1}. Thus, E_α at various α_i for AP with and without nanocrystals ($CdFe_2O_4$ and Cd) have been evaluated and the E_α dependencies are shown in Fig. 7.

4.2. Ignition delay measurements

The ignition delay (D_i) measurements were undertaken using the tube furnace (TF) [18] in the temperature range of 360–420 °C

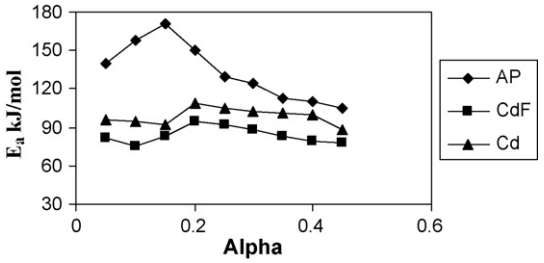

Fig. 7. Dependencies of activation energy on the extent of conversion α.

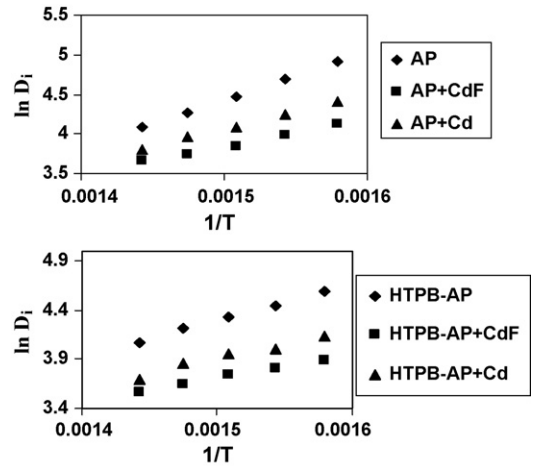

Fig. 8. Graph of $\ln D_i$ vs. $1/T$ (a) for nanocrystals with AP and (b) for nanocrystals with AP-HTPB.

(±1 °C). 20 mg of samples (AP and CSP with and without nanocrystals in same ratio as in TG) were taken in an ignition tube and time interval between the insertion of the ignition tube into the TF and the moment of ignition indicated by the appearance of fumes with light, gave the value of ignition delay in seconds. The sample was inserted into the TF with the help of a bent wire. The time for the insertion of the ignition tube into the TF was kept constant throughout each run. The accuracy of temperature measurements of TF was ±1 °C. Each run was taken five times and mean D_i value are reported in Table 3. The D_i data were found to fit in the Eq. (6) [19–22]

$$D_i = A \exp\left(\frac{E_a^*}{RT}\right) \tag{6}$$

where E_a^* is the activation energy for ignition, A is the pre-exponential factor and T the absolute temperature. E_a^* assessed by above equation along with the correlation coefficient (r) are given in Table 3. Plots of D_i vs. $1/T$ are presented in Fig. 8(a and b).

4.3. Burning rate measurements

The burning rate of propellants was measured at ambient pressure by fuse wire technique [14]. An average of 3 measurements was taken within experimental error and results are reported in Table 3.

5. Results and discussion

The XRD characterization of nanocrystals suggests its purity as shown in Fig. 1. The peaks of $CdFe_2O_4$ and Cd nanocrystals are very intensive and sharp. The diffraction data are in good agreement with JCPDS card of $CdFe_2O_4$ (JCPDS No. 22-1063) and Cd (JCPDS No. 05-0674). The average size of $CdFe_2O_4$ and Cd nanocrystals are estimated to be 14.9 and 8.8 nm, respectively. TEM micrographs

Table 1
Crystal size of $CdFe_2O_4$ and Cd.

Nanocrystal	Particle size (nm)	
	XRD	TEM
$CdFe_2O_4$	14.9	12.5
Cd	8.8	10

Table 2
Burning rate of HTPB-AP CSPs with and without $CdFe_2O_4$ and Cd nanocrystals.

Additive	Burning rate (mm/s)	rb/rb*
Nil	1.15	1.00
$CdFe_2O_4$	1.94	1.69
Cd	1.62	1.41

rb and rb* = burning rate of propellant with and without nanocrystals, respectively.

show very narrow particle size distribution with mean diameter of ~12.5 nm for $CdFe_2O_4$ (Fig. 2a and b) and ~10 nm for Cd (Fig. 2c and d) which is in good agreement with that estimated by Scherrer equation [23,24] from the XRD pattern (Table 1).

Results reported in Table 2 shows that burning rate of CSPs is enhanced on incorporation of $CdFe_2O_4$ and Cd as catalyst. Increase of burning rate might be due to the enhanced decomposition of AP or HTPB or CSP. In order to find out which of the above processes is accelerated, TG, TG-DSC and ignition delay of AP, HTPB, CSP with and without catalysts were studied.

TG curve (Fig. 3) for AP with $CdFe_2O_4$ and Cd confirm beyond doubt that nanocrystals affect both low temperature decomposition (LTD) and high temperature decomposition (HTD) of AP. Incorporation of catalyst not only increase the rate of mass loss but also lower the HTD of AP, to form gaseous products.

The DSC curve (Fig. 3) also verifies the results obtained from TG. DSC curve for AP (Fig. 3a) has apparently three stages. In the first stage, the endothermic peak appears at 242 °C, ascribed to its transition from orthorhombic to cubic form [25]. In the second stage, the exothermic peak at 310 °C is attributed to the partial decomposition of AP and the formation of intermediate products. The third main exothermic peak appears at relatively higher temperature of 430 °C, indicating complete decomposition of the intermediate products. As the catalysts were added to AP, the endothermic peak appears at 242 °C, indicating that catalysts have no effect on the crystallographic transition temperature but noticeable changes were observed in first and second exothermic peaks. When $CdFe_2O_4$ was added to the AP, only one exothermic peak appeared at about 320 °C (Fig. 3b) but when Cd was added to the AP, the first exothermic peak shifted from 310 to 290 °C and the second exothermic peak shifted from 430 to 400 °C (Fig. 3c).

From Fig. 4, it is clear that the rate of HTPB decomposition is enhanced when catalysts were added, which may be due to increase in oxidative degradation [26]. It is also known that traces of metals catalyze the homolytic decomposition of hydroperoxides which are formed during oxidative degradation of the HTPB [27].

The rate of decomposition of CSPs is enhanced in presence of $CdFe_2O_4$ and Cd due to the large number of defects and dislocations in the crystal lattice of nanocrystals. Thus a large number of active sites would be available for the adsorption of reactants; as a consequence, the rate of reaction would be increased. Ferrite spinels may also contain mixture of two divalent metal ions. The cation distribution of ferrites significantly affects the surface properties making them catalytically active. Moreover, studies have also suggested that ballistic modifiers are active mainly in the condense phase at AP-binder interface [28]. TG curves shown in Fig. 4 indicate that the condensed phase reactions are occurring in CSPs. Thus catalysts affect all the three processes, viz., decomposition of the HTPB, oxidizer (AP) and propellants (CSPs).

The effects of $CdFe_2O_4$ and Cd nanocrystals on the thermolysis of AP by varying their amount (Fig. 5) clearly show that increase of catalyst may increase the thermal decomposition of AP. From Table 3, it is clear that both ignition delay and the activation energy for ignition of AP and CSPs are lowered by $CdFe_2O_4$ and Cd nanocrystals in the temperature range of 360–420 °C.

The set of reaction models (Table 4) [16,29] were used to analyze isothermal TG data (in the range 300–340 °C, Fig. 5) to calculate the E_a values for thermal decomposition of AP and AP in presence of $CdFe_2O_4$ and Cd (1% by wt). The activation energy values are reported in Table 5. In the model fitting method, the kinetics is analyzed by choosing a "best fit" model based on the value of the correlation coefficient '*r*' close to 1. Among the various values of *r*, calculated for different models, the highest value of r for AP corresponds to model 13 and AP with $CdFe_2O_4$ and Cd corresponds to model 11 and 5. The corresponding values of E_a were reported for AP, AP + $CdFe_2O_4$ and AP + Cd are, respectively, 102.0, 65.8 and 83.7 kJ mol^{-1} (Table 5).

Ignition delay (D_i) actually is the time interval between the insertion of the ignition tube (having sample) into the tube furnace and the moment of an ignition. The ignition-delay measurements in the temperature range 360–420 °C for AP and HTPB-AP with and without nanocrystals have been carried out. It has been experimentally observed that values of D_i (of sample studied) falls as the temperature increases. Further, incorporation of a nanocrystal ($CdFe_2O_4$ and Cd) cause decrease of energy of activation for ignition (D_i).

The isoconversional method [17] is known to permit estimation of the apparent activation energy independent of the model, corresponding to the extent of conversion of the sample. According to Fig. 6, each activation energy has a separate value at different αs. The value of E_a of AP is higher than that of AP with $CdFe_2O_4$ and Cd. Nevertheless, a new computational technique (advance isoconversional method) has been used by Vyazovkin and Wight [30] to determine the dependence of the effective activation energy (E_α) on α for isothermal TG data. They have suggested that the initial decomposition ($\alpha \to 0$) of cubic AP shows the activation energy of 90 kJ mol^{-1} for the isothermal decomposition and 130 kJ mol^{-1} for the non-isothermal decomposition. The difference in activation energy could be due to nucleation and nuclei growth, respectively, for isothermal and non-isothermal decompositions.

Table 3
Ignition delay (D_i), activation energy for ignition (E_a) and correlation coefficient of AP and CSP with and without $CdFe_2O_4$ and Cd nanocrystals.

Sample	D_i (s)					E_a^* (kJ/mol)	*r* (correlation coefficient)
	360 ± 1 °C	375 ± 1 °C	390 ± 1 °C	405 ± 1 °C	420 ± 1 °C		
AP	135	108	88	71	60	49.7	0.9996
AP + $CdFe_2O_4$(1%wt)	62	54	47	42	39	28.6	0.9959
AP + Cd(1%wt)	83	70	60	51	45	36.5	0.9991
HTPB-AP	99	85	76	68	59	30.6	0.9983
HTPB-AP + $CdFe_2O_4$ (1%wt)	49	45	42	38	35	20.4	0.9937
HTPB-AP + Cd (1%wt)	62	55	52	47	40	25.0	0.9839

Table 4
Set of reaction models applied to describe thermal decomposition of solids.

Model no.	Reaction model	$f(\alpha)$	$g(\alpha)$
1.	Power law	$4\alpha^{3/4}$	$\alpha^{1/4}$
2.	Power law	$3\alpha^{2/3}$	$\alpha^{1/3}$
3.	Power law	$2\alpha^{1/2}$	$\alpha^{1/2}$
4.	Power law	$2/3\alpha^{-1/2}$	$\alpha^{3/2}$
5.	One-dimensional diffusion	$1/2\alpha^{-1}$	α^{2}
6.	Mampel (first order)	$1-\alpha$	$-\ln(1-\alpha)$
7.	Avrami-Erofeev	$4(1-\alpha)[-\ln(1-\alpha)]^{3/4}$	$[-\ln(1-\alpha)]^{1/4}$
8.	Avrami-Erofeev	$3(1-\alpha)[-\ln(1-\alpha)]^{2/3}$	$[-\ln(1-\alpha)]^{1/3}$
9.	Avrami-Erofeev	$2(1-\alpha)[-\ln(1-\alpha)]^{1/2}$	$[-\ln(1-\alpha)]^{1/2}$
10.	Contracting sphere	$3(1-\alpha)^{2/3}$	$1-(1-\alpha)^{1/3}$
11.	Three-dimensional diffusion	$2(1-\alpha)^{2/3}[1-(1-\alpha)^{1/3}]^{-1}$	$[1-(1-\alpha)^{1/3}]^{2}$
12.	Contracting cylinder	$2(1-\alpha)^{1/2}$	$1-(1-\alpha)^{1/2}$
13.	Prout-Tompkins	$\alpha/(1-\alpha)$	$\ln(\alpha/1-\alpha)$
14.	Ginstling-Brounshtein	$3/2[(1-\alpha)^{-1/3}-1]^{-1}$	$[1-(2\alpha/3)]-(1-\alpha)^{2/3}$

Table 5
Activation energy (E_a), Arrhenius parameters and correlation coefficient (r) for the isothermal decomposition of AP and AP with $CdFe_2O_4$ and Cd.

Model	AP			AP+$CdFe_2O_4$			AP+Cd		
	E_a (kJ mol^{-1})	$-\ln A$	r	E_a (kJ mol^{-1})	$-\ln A$	r	E_a (kJ mol−)	$-\ln A$	r
1	94.7	13.8	0.9619	59.3	7.4	0.9156	78.6	11.3	0.9954
2	95.0	14.1	0.9622	59.5	7.6	0.9171	78.8	11.4	0.9956
3	95.6	14.3	0.9627	60.2	7.9	0.9232	79.4	11.7	0.9960
4	98.4	14.6	0.9646	63.4	8.3	0.9349	82.4	12.0	0.9973
5	99.4	14.4	0.9648	64.8	8.2	0.9403	83.7	11.9	0.9977
6	98.0	15.1	0.9641	62.9	8.7	0.9329	82.0	12.5	0.9971
7	97.0	14.6	0.9646	61.3	8.1	0.9250	80.5	11.8	0.9967
8	95.6	14.4	0.9626	60.3	8.0	0.9209	79.5	11.7	0.9960
9	96.3	14.7	0.9631	61.0	8.4	0.9242	80.2	12.1	0.9963
10	97.7	13.8	0.9640	62.6	7.5	0.9314	81.6	11.2	0.9961
11	100.2	12.8	0.9625	65.8	6.5	0.9436	84.9	10.3	0.9611
12	97.6	14.2	0.9640	62.4	7.8	0.9306	81.4	11.5	0.9970
13	102.0	17.5	0.9801	59.4	9.5	0.9164	86.2	14.8	0.9736
14	88.5	10.3	0.9288	65.4	6.3	0.9425	70.8	7.3	0.9675

Isoconversional kinetic analysis has also been carried out by Lang and Vyazovkin [31] to detect changes in the effective activation energy of the thermal decomposition of AP by using DSC, TGA, and high pressure DSC (HP-DSC) techniques. It has been reported that the initial stages of decomposition characterize by a change in the effective activation energy from ∼100 to ∼60 kJ mol^{-1}. It is inferred that solid AP decompose via two major channels, endothermic sublimation and exothermic surface reaction of sublimation products. In addition, model free and model fitting approaches to kinetic analysis of isothermal and non-isothermal decomposition of HMX and ammonium dinitramide have also been reported in detail [32] by applying an *F*-test to check the significance of the difference of different kinetic models.

A number of reactions have been reported [33,34] to be involved in the decomposition and combustion of AP because of the four elements and the full range of oxidation states utilized by nitrogen and chlorine. The breaking of an N–H bond, then proton transfer from NH_4^+ to ClO_4^- to form an O–H bond leads to the formation of NH_3 and $HClO_4$ in a primary step in condense phases [35]. Further secondary reactions occur at higher temperature through complex competitive steps to produce gaseous products.

6. Conclusions

$CdFe_2O_4$ and Cd nanocrystals were prepared and characterized by XRD and TEM. These show good catalytic effect on the thermal decomposition of AP, HTPB and CSPs, though $CdFe_2O_4$ is better than that of the Cd nanocrystals. The burning rate of CSPs was also found to be enhanced. Though model fitting method using a set of reaction model applied to isothermal data but model free approach (isoconversional method) is a better method of obtaining reliable and consistent kinetic information.

Acknowledgements

The authors are grateful to Head, Chemistry Department of DDU Gorakhpur University for laboratory facility; IIT Roorkee for TG-DSC; STIC, Cochin for XRD and Punjab University for TEM images. Thanks are also due to financial assistance by CSIR for providing Emeritus Scientist to G. Singh, JRF to Reena Dubey and RA to Dr. Pratibha Srivastava.

References

[1] D.S. Mathew, R.-S. Juang, Chem. Eng. J. 129 (2007) 51.
[2] H. Gleiter, Prog. Mater. Sci. 33 (1989) 223.
[3] J.H. Fendler, Chem. Rev. 87 (1987) 877.
[4] M. Samim, N.K. Kaushik, A. Maitra, Bull. Mater. Sci. 30 (2007) 535.
[5] Y. Li, L. Li, H. Liao, H. Wang, J. Mater. Chem. 9 (1999) 2975.
[6] S. Wu, D. Chen, J. Colloid Interface Sci. 259 (2003) 282.
[7] Z. Gui, R. Fan, W. Mo, X. Chen, L. Yang, Y. Hu, Mater. Res. Bull. 38 (2003) 169.
[8] S. Verma, P.A. Joy, Y.B. Khollam, H.S. Potdar, S.B. Deshpande, Mater. Lett. 58 (2004) 1092.
[9] Z. Tianshu, P. Hing, Z. Jiangchang, K. Lingbing, Mater. Chem. Phys. 61 (1999) 192.
[10] G. Singh, I.P.S. Kapoor, S. Dubey, P.F. Siril, J.H. Yi, F.-Q. Zhao, R.-Z. Hu, Thermochim. Acta 477 (2008) 42.
[11] H. Duan, X. Lin, G. Liu, L. Xu, F. Li, J. Mater. Prrocess. Tech. 208 (2008) 494.
[12] S.-H. Wu, D.-H. Chen, J. Colloid Interface Sci. 259 (2003) 282.
[13] S. Krishna, R.D. Swami, J. Propul. Power 13 (2) (1997) 207.
[14] G. Singh, S.P. Felix, Combust. Flame 132 (2003) 422.
[15] G. Singh, R.R. Singh, Res. Ind. 23 (1978) 92.
[16] M.E. Brown, D. Dollimore, A.K. Galway, Compr. Chem. Kinet. 22 (1960).
[17] S.V. Vyazovkin, Int. J. Chem. Kinet. 28 (1996) 95.
[18] G. Singh, S.K. Vasudeva, I.P.S. Kapoor, Indian J. Tech. 29 (1991) 589.

[19] N. Semenov, Chemical Kinetics and Chain Reactions, Clarendon Press, Oxford, UK, 1935, p. 18.
[20] E.S. Freeman, S. Gordon, J. Phys. Chem. 60 (1956) 867.
[21] J. Zinn, R.N. Rogers, J. Phys. Chem. 66 (1962) 2646.
[22] G. Singh, R.R. Singh, A.P. Rai, I.P.S. Kapoor, J. Therm. Anal. 36 (1990) 2539.
[23] X. Lu, X. Wang, J. Zhang, X. Lu, L. Lu, Thermochim. Acta 342 (1999) 97.
[24] L.S. Birks, H. Friedman, J. Appl. Phys. 17 (1946) 687.
[25] V.V. Boldyerv, Thermochim. Acta 443 (2006) 1.
[26] R.P. Rastogi, G. Singh, B.L. Dubey, C.S. Shukla, J. Catal. 65 (1980) 25.
[27] P. Srivastava, I.P.S. Kapoor, G. Singh, J. Alloys Compd. 485 (2009) 88.
[28] S.R. Chakravarthy, E.W. Price, R.K. Sigman, J. Propul. Power 13 (1997) 471.
[29] I.P.S. Kapoor, P. Srivastava, G. Singh, U.P. Singh, R. Frohlich, J. Phys. Chem. A 112 (2008) 652.
[30] S. Vyazovkin, C.A. Wight, Chem. Mater. 11 (1999) 3386.
[31] A.J. Lang, S. Vyazovkin, Combust. Flame 145 (2006) 779.
[32] S. Vyazovkin, C.A. Wight, Thermochim. Acta 340–341 (1999) 53.
[33] W.A. Rosser, S.H. Inami, Combust. Flame 12 (1968) 427.
[34] N.E. Ermolin, O.P. Korobeinchev, A.G. Tereshenk, V.M. Foomin, Combust. Explos. Shock Waves 18 (1982) 180–189.
[35] G. Singh, I.P.S. Kapoor, D.K. Pandey, J. Energy Mater. 20 (2002) 223.